



Optimization of sol–gel based ZnO metal–semiconductor–metal UV detectors by Zr doping through sputtering method

Nader Madani-Mashaei¹ · Ebrahim Asl Soleimani^{1,2} · Hamidreza Shirvani-Mahdavi¹

Received: 7 December 2020 / Accepted: 4 February 2021 / Published online: 25 February 2021
© The Author(s), under exclusive licence to Springer-Verlag GmbH, DE part of Springer Nature 2021

Abstract

In this study, to improve the properties of ZnO-based metal–semiconductor–metal (MSM) UV detectors, the surface of ZnO thin films prepared by the sol–gel method is initially doped with Zr sputtering at different time intervals. The amount of Zr at the surface and its effect on the crystalline structure and the surface morphology are, respectively, evaluated through energy-dispersive X-ray spectroscopy (EDX), X-ray diffraction (XRD) analysis, and atomic force microscopy (AFM). Then, by creating electrodes on the surface, these layers are converted to MSM UV detectors and subjected to various sensor tests to assess their performance. The results of these tests show that the sensors, which are sputtered with Zr for 50 s under the experimental conditions in question, experience an increase in the photoresponsivity by about one order of magnitude while their rise time and recovery time decrease about 30%. Furthermore, the best repeatability of $I-t$ curves and baseline stability in consecutive cycles are also related to these sensors. The experience also indicates that the use of sputtering method can be seriously considered to modify the surface of nanostructures used in the construction of sensors. This makes perfect sense because the surface plays a major role in the detection mechanisms in most light and gas sensors. It is noteworthy that this method can be used even to modify the properties of pre-made detectors.

Keywords ZnO thin film · MSM UV detector · Sol-gel process · Sputtering method · Response time

1 Introduction

Nowadays, ultraviolet light detection is of significant importance in many aspects of science and technology associated with health, environment, and space applications such as flame monitoring, water purification system, chemical agent detection, space communications and ozone layer monitoring [1–4]. Semiconductor materials have always shown a great promise for photodetectors because of their cheapness and simplicity. One of these materials is ZnO, which has received serious attention for fabricating UV detectors owing to having a bandgap of 3.37 eV and a large excitation energy of 60 meV. ZnO is an abundant, inexpensive, and non-toxic material, which exhibits high thermal and chemical stability in harsh environments [5–7].

Different factors such as construction technique, type of photodetector [8], the material and shape of electrodes, type of electrodes' connection [9–11], and doping method seriously impact on the performance of detectors. The incorporation of foreign dopant ions into ZnO nanostructures is an approach widely used to change their electrical, optical, and photoconductive properties [12–22]. In thin layers of ZnO, the presence of dopant atoms in the form of replacement with ions, interstitial, and segregated in grain boundaries can make dramatic changes in the concentration of carriers, the mobility, and the resistivity and also form new bondings and energy levels, which in turn cause great changes in the electrical, optical, and chemical properties of semiconductors. By selecting one of appropriate doping ways, the type, and the amount of dopant, one can improve the characteristics of sensors made by these layers and manage for the intended purpose.

To improve ZnO performance in various applications, diverse metallic dopants including aluminum (Al) [13, 14], cobalt (Co) [15, 16], silver (Ag) [17, 18], copper (Cu) [19, 20], and titanium (Ti) [21, 22] have been exploited. Zr similar to some other elements, owing to its positive and

✉ Ebrahim Asl Soleimani
Ebr.Asl_Soleimani@iauctb.ac.ir

¹ Department of Physics, Central Tehran Branch, Islamic Azad University, Tehran, Islamic Republic of Iran

² Department of Electrical and Computer Engineering, University of Tehran, Tehran, Islamic Republic of Iran

important effects on improving the performance of ZnO, has been also widely studied [23–33]. Nevertheless, in this case, it appears that there are many other worthy properties and effects that could be investigated.

In this research work, to improve sensor properties of ZnO thin layers, these films are initially sputtered with Zr at different interval times. Then, the presence of dopant and its effects on the structure of layers are examined through EDX spectroscopy, AFM, and XRD analysis. In the next step, by creating electrodes on the surface of the layers, their characteristics as ultraviolet sensors are studied. The measurements indicate that, by the selection of appropriate conditions of sputtering, the response time of the UV detectors of the type of MSM made by these layers can be optimized. Some advantages of this approach are its simplicity and speed; furthermore, it can be used to improve the performance of pre-made detectors.

2 Experimental

First, several pure zinc oxide layers were provided by spin coating method, and then, some of them were doped by Zr through sputtering technique. A number of the samples doped by Zr were subjected to structural tests, and for conducting sensor tests, the process of electrode placement was performed on the other similar samples. The details of preparation and testing the samples are described as follows.

2.1 Sample preparation

Soda lime glass substrates were initially cleaned with acetone and deionized water, and then, for further cleaning and pre-preparation of the glass surface it was heated up to 500 °C for 1 h. Zinc acetate dihydrate, isopropanol, and monoethanolamine (MEA) were used as the starting material, solvent, and stabilizer, respectively. The molar ratio of MEA to zinc acetate was maintained at 1, and the concentration of zinc acetate was selected equal to 0.5 M. Zinc acetate dihydrate was first dissolved in isopropanol, and the solution was stirred at room temperature at 500 rpm. After 1 h when the solution turned milky, MEA was added drop by drop to yield a clear transparent homogeneous solution, and then, the resulting mixture was stirred at 60 °C for 1 h. After aging for 48 h, the solution was deposited on the cleaned substrates by the spin coating method at room temperature, with a rate of 2000 rpm for 25 s. Having coated the samples, they were heated at 250 °C in air for 10 min to evaporate the solvent and remove the residual of organic materials. The coating and drying procedures were repeated three times to increase the film thickness. Finally, all the samples were annealed in ambient atmosphere at 500 °C temperature for 1 h. In addition, the thickness of the films was measured

equal to 405 ± 16 nm through calculating the mass change of samples due to coating. To achieve more accurate result, the above thickness was obtained from averaging of the results related to 15 coated samples. In the next step, the surface of samples was doped through the sputtering technique using a Zr bulk with purity of 99.99% as a target. The experimental conditions, except for the sputtering time, were considered the same for all samples. The distance of all samples from the target, the current, the voltage, and the argon pressure were selected equal to 8 cm, 25 mA, 100 V, and 0.06 mbar, respectively. But, the sputtering time was taken into account different and between 25 and 3200 s.

2.2 Examination of the layers structure

In each of the above sputtering times, several doped samples were provided. First, the existence and the value of Zr on the surface of the layers were examined through EDX spectroscopy. Then, the effect of the presence of Zr atoms on the surface and the crystalline structure was studied by AFM and XRD spectroscopy, respectively. To fabricate a detector from each group of the similar samples with identical doping, two electrodes were placed by the method of thermal evaporation on the surface of each of the samples. It should be noted that the electrodes were made from copper in the form of two semicircles with the diameters of 5 mm and the thicknesses of about 100 nm. The semicircles have been separated by a distance of 200 microns so that they virtually form a circle with the diameter of 5 mm with a gap of 200 microns in the diameter. In addition, for better repeatability of the results, two completely similar detectors were made on the surface of each sample (Fig. 1).

2.3 Functional test of sensors

The principal features of the fabricated sensors involving the response time, the photoresponsivity, the sensitivity, the dark current, and the UV photocurrent were determined by the use of the $I-t$ curves for all sensors, which were drawn under UV light exposure (with a periodicity of 100 s) and a 4 V bias voltage. It should be noted that the dark current and the photocurrent for all sensors have



Fig. 1 An example of similar UV dual sensors fabricated in this research

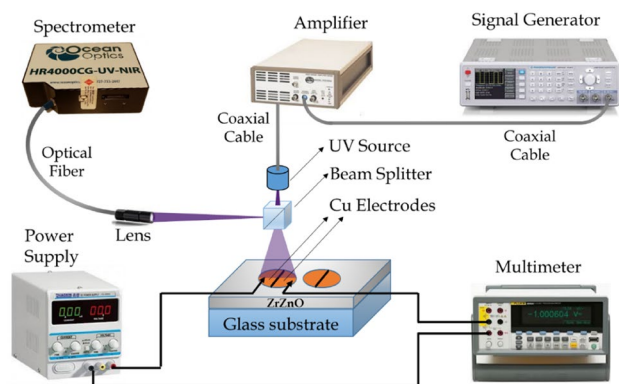


Fig. 2 A schematic setup for testing the fabricated MSM UV sensors. The power of UV light source in the sensor predetermined location is measured by the MAESTRO power and energy meter with the low-power thermopile XLP12 (from gentec-eo Co.) before placing the sensor there. The amplifier (model PZD 350A from Trek Co.) has been used to provide the power of UV source. The wavelength band of the beam splitter is in the range of UV light

been specified based on the minimum current at the first cycle (before the first exposure) and the maximum current at the second cycle (during the UV light radiation), respectively. Figure 2 shows a schematic setup through which testing the fabricated sensors is performed. The LED-type UV light source with the wavelength 370 nm and the full width at half maximum (FWHM) 30 nm generates a power equal to 0.6 mW in the sensor location. The wavelength of the light source and its power in the sensor location were measured by the spectrometer HR4000 (from Ocean Optics Co.) and the MAESTRO power and energy meter with the low-power thermopile XLP12 (from gentec-eo Co.), respectively. The LED power is supplied by an accurate function generator HMF2550 (from Hameg Co.), and the current measurement is performed by a precision 6.5 digit multimeter 8846 A (from Fluke Co.). To reduce the noise, the setup

was entirely placed in the metallic chamber connected with the earth.

3 Results and discussion

To evaluate the extent of Zr on the surface and its effect on the crystalline structure and the surface morphology, EDX spectroscopy, XRD analysis, and AFM were carried out for two outermost samples, one without Zr (sample a) and the other doped with Zr by sputtering technique in a duration of 3200 s (sample g).

Using the EDX spectrum of the sample g (Fig. 3a), Zr-to-Zn atomic ratio of this sample was obtained equal to 0.046. Taking into account sputtering-induced morphologies, it is generally expected that Zr-dopant atoms place on the surface and have a small penetration depth in the ZnO layer. Hence, since the main mechanism of this type of detectors sets on the surface, the use of the sputtering technique can be considered as an advantage. The other peaks being in the spectrum, as seen from the pure substrate spectrum (Fig. 3b), are obviously related to the substrate.

In the XRD spectrum of sample a, two peaks at the deviation angles of 34.67° and 63.11° are, respectively, in good agreement with the (002) and (103) planes of the ZnO wurtzite hexagonal (Fig. 4a). Two similar peaks but with a slight decrease in their deviation angles are also observed at the positions of 34.60° and 63.02° in sample g (Fig. 4b). The existence of two peaks in the spectra and whose low intensities indicate that the structure of layers is polycrystalline. In addition, after sputtering of Zr, the intensity of the peaks decreases, while their FWHM increases. One important reason of the above variations can be more disorder of the crystalline structure due to the presence of the Zr atoms. As expected, due to the relatively low percentage of Zr and the way of its doping which causes most of it to place on the surface, the changes generated in the crystalline structure

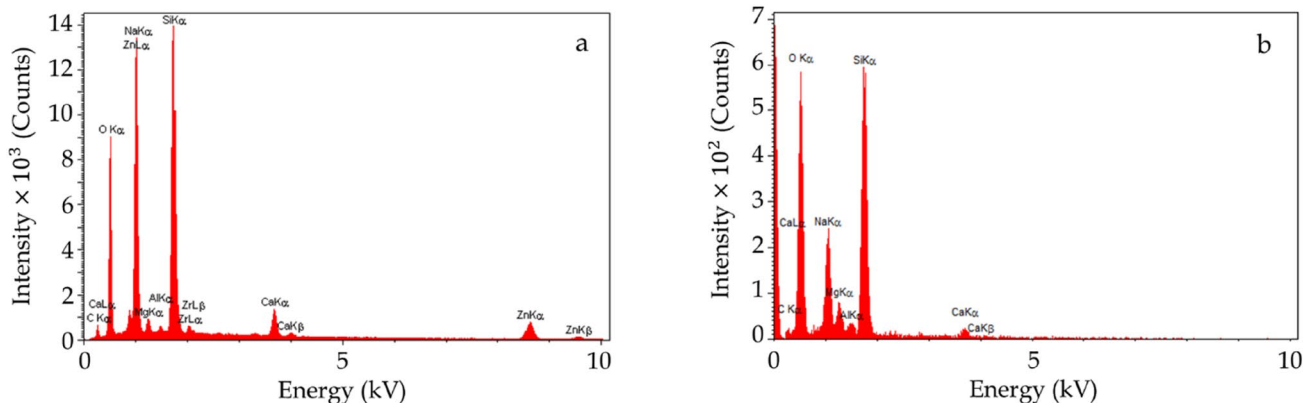


Fig. 3 EDX spectra of **a** the sample g sputtered with Zr for 3200 s and **b** the pure substrate

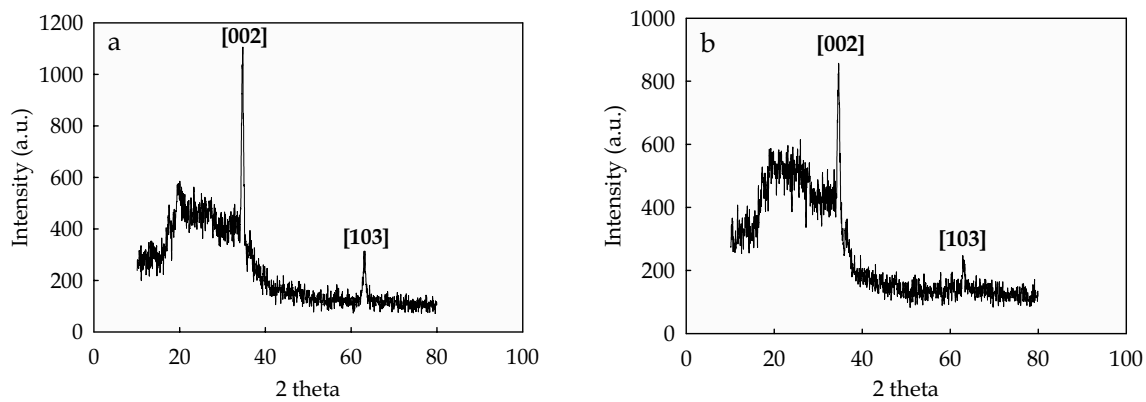


Fig. 4 XRD spectra of **a** the pure zinc oxide layer and **b** the sample *g* sputtered with Zr for 3200 s

are not dominant even for the layer with the maximum sputtering time (3200 s). In the event that the variations of the electrical parameters of the fabricated sensors using these samples, as will be discussed in the later sections, are considerable even for the sample with the minimum sputtering time (25 s).

The role of Zr in the microstructures and surface roughness of the films can be evaluated by comparing the maximum peak to valley heights (*PVH*) related to the samples before and after doping. The measurements for different surface areas of the undoped sample and the sample doped with Zr for 3200 s sputtering indicate that the value of *PVH* reduces from 52.6 to 34.3 nm.

As seen from Fig. 5, grains have spherical shape in both samples, and the diameter average of most of them is about 50 nm, though smaller and larger grains are also observable. The comparison of the sample of pure ZnO with that has been sputtered with Zr during 3200 s indicates that even

the most time of sputtering with Zr has not created serious change in the grains' shape and size. The only observable change is that the average roughness has decreased from 5.8 to 3.9 nm, which can mean the placement of Zr atoms in the porous space between the grains, and to some extent being filled this porous space. This consequence is expectable, since unlike other doping methods in which the presence of dopants during the growth process affects the formation of grains, in the sputtering method, dopant as a coating affects more on the outer surface of the layer.

Figure 6 indicates the photoluminescence (PL) spectra obtained for the undoped and doped (for 3200 s sputtering) samples. Here, the wavelength of exciting light is 270 nm. The quality of the layers due to surface defect states can be evaluated by these spectra. As seen from Fig. 6, after Zr doping by the sputtering method, no significant change occurs in the near band-edge; in this region, the peak is corresponding to excitonic emissions [9], whereas the blue emission peak

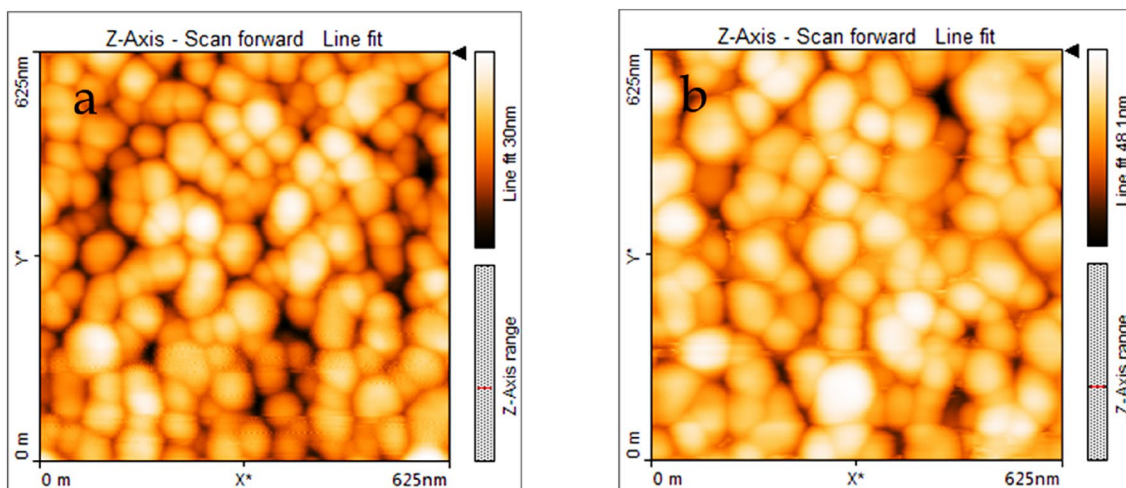


Fig. 5 AFM surface morphology images of **a** the pure zinc oxide layer and **b** the sample *g* sputtered with Zr for 3200 s

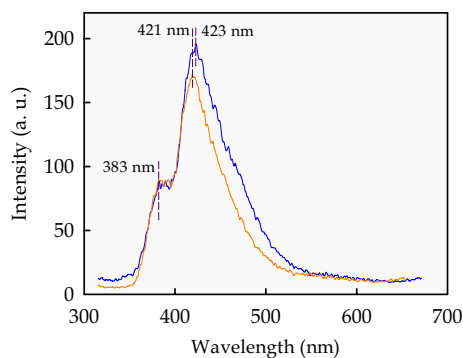


Fig. 6 Photoluminescence (PL) spectra of undoped and doped (for 3200 s sputtering) samples. The wavelength of exciting light is 270 nm. Blue color: undoped sample; orange color: doped sample

at the wavelength 423 nm is reduced and partially shifted toward shorter wavelengths. This peak considering its great width can be attributed to defects related to oxygen interstitial, zinc vacancy, and oxygen vacancy and even the recombination of free excitons [10, 34]. Therefore, reducing the amplitude of this peak means reducing the above defects in the layer as well as reducing the recombination of free excitons. This is while that in other common methods of doping, entering Zr into ZnO causes an increase in defects of these types [31]. The weak emission in the rest of visible region indicates low defects and acceptable quality of layers, which can be used to fabricate UV sensors.

The change of the electrical characteristics of the zinc oxide layers affected by Zr doping has previously been reviewed thoroughly [24–26, 28, 33, 35], but the response time of the sensors fabricated using these layers has not accurately studied yet; even if it was mentioned, it was not the main goal of the study. In this study, although examining the response time change of the detectors in the presence of Zr is the pivotal issue, the following parameters have also been taken into investigation: (1) The maximum current under UV illumination (I_i) and the dark current (I_d), (2) photoresponsivity, $R \equiv I_{ph}/P_{op}$, where $I_{ph} = I_i - I_d$ is the photocurrent and P_{op} is the incident optical power, (3) the sensitivity, $S \equiv I_{ph}/I_d$. For this purpose, $I-t$ curve was plotted for six different detectors sputtered with Zr in various sputtering times and the non-sputtered sample as per what was mentioned in the experimental section (Fig. 7). Table 1 indicates the results obtained from the curves of Fig. 7 for the above-mentioned parameters of the sensors. As seen, these parameters significantly change by entering Zr atoms on the surface of ZnO films. In high-doped sensors, in $I-t$ curves, at the moments of turning on and off the UV light, the process of changing the current in each cycle is first accelerated and then slowed down. The initial rapid increase or decrease in the current can be explained as follows. When the UV light turns on, by generating electron

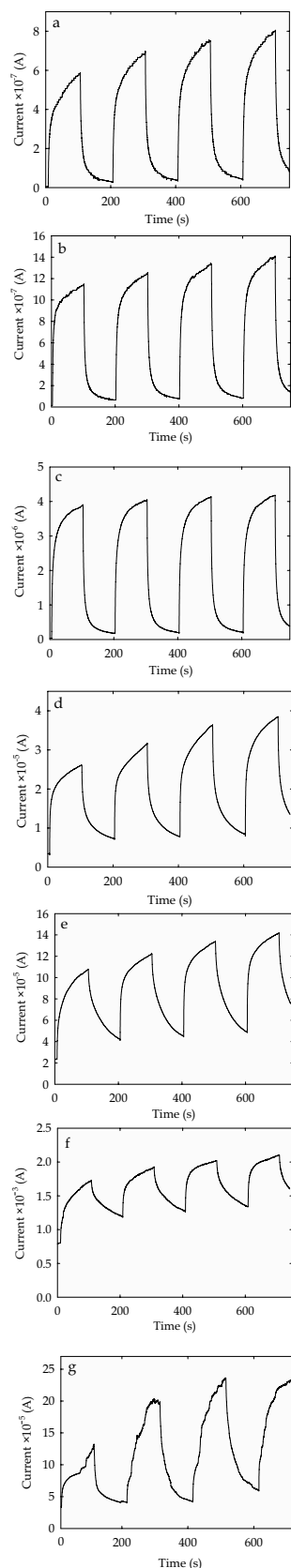


Fig. 7 $I-t$ curves of the sensors fabricated from **a** the pure zinc oxide layer and ZnO layers sputtered with Zr for **b** 25 s, **c** 50 s, **d** 200 s, **e** 800 s, **f** 1600 s, and **g** 3200 s

Table 1 The quantities measured related to the samples, t_s : sputtering time; $R.T.$: rise time; $F.T.$: fall time; R : responsivity; S : sensitivity; I_d : dark current; I_i : the maximum current under UV illumination

Sample	t_s (s)	$R.T.$ (s)	$F.T.$ (s)	R (A/W)	S	I_d (μ A)	I_i (μ A)
<i>a</i>	0	49	6.5	58	68.40	0.010	0.694
<i>b</i>	25	44	6.1	101	19.49	0.061	1.250
<i>c</i>	50	34	4.3	310	9.67	0.378	4.033
<i>d</i>	200	57	35.1	2388	8.19	3.431	31.541
<i>e</i>	800	65	> 1000	7986	4.01	23.468	117.459
<i>f</i>	1600	25	> 1000	96,878	1.45	785.112	1925.372
<i>g</i>	3200	75	19.0	13,911	4.56	35.907	199.644

holes and recombining the holes with electrons of oxygen ions which, in the early moments, are accumulated on the surface, the release of these ions is quickly performed. This in turn causes a rapid increase in current in the initial moments. As the number of oxygen ions on the surface decreases, their rate of separation (which is proportional to the rate of increase in current) decreases exponentially. By turning off the UV light, this process is reversed, i.e., at first, when the presence of oxygen ions on the surface is negligible, oxygen readsorption rapidly occurs in effect of the multiplicity of additional electrons caused by the dopants. Then, with the accumulation of oxygen ions on the surface, the rate of adsorption (which is proportional to the rate of current reduction) gradually exponentially slows down. It should be noted that this phenomenon can also be present in undoped samples. However, in the doped samples owing to the formation of new bondings and significant increase in carriers, and consequently, serious increase in the amount of adsorbed and desorbed oxygen by turning the UV light on and off repeatedly, this phenomenon is more intensely and clearly observable.

Figure 8a, b shows curves of the variation of the dark current and the maximum photocurrent as a function of the sputtering time, respectively, when the UV light is off and on. As it can clearly be observed, by increasing the sputtering time (which means an enhancement of Zr amount) up to

1600 s, the currents increase, and then, there is a decreasing trend. The reason for the increase in current up to 1600 s can be attributed more to the replacement of Zr^{4+} ions instead of Zn^{2+} and to some extent the presence of Zr atoms interstitially in the space between the lattice atoms, which in turn increases the carriers [25, 26, 35–37]. To justify the reduction of the currents of sample g, which has been sputtered for the 3200 s (the maximum time), it should be noted that with increasing sputtering time, the possibility of Zr atoms interstitially in the space between lattice atoms and also their segregation at the surface, especially at the grain boundaries, can be increased. In this case, increasing the presence of Zr atoms interstitially causes irregularities in the crystal lattice, and their segregation, which can lead to the formation of neutral zirconium atoms and reduction of carriers, makes more dispersion of carriers at the grain boundaries. Furthermore, both of these effects reduce the carriers' mobility and enhance the electrical resistance. By increasing the amount of Zr, in addition to the above influences, the scattering phenomenon due to the presence of ionized dopants will also help reduce the mobility and increase the resistance. Similar to this phenomenon that with entering low values of dopant in ZnO thin films, at first the conductance increases and then decreases by increasing the value of dopant, has been previously also reported for zirconium and some other metallic dopants [25–27, 33, 36, 38–40].

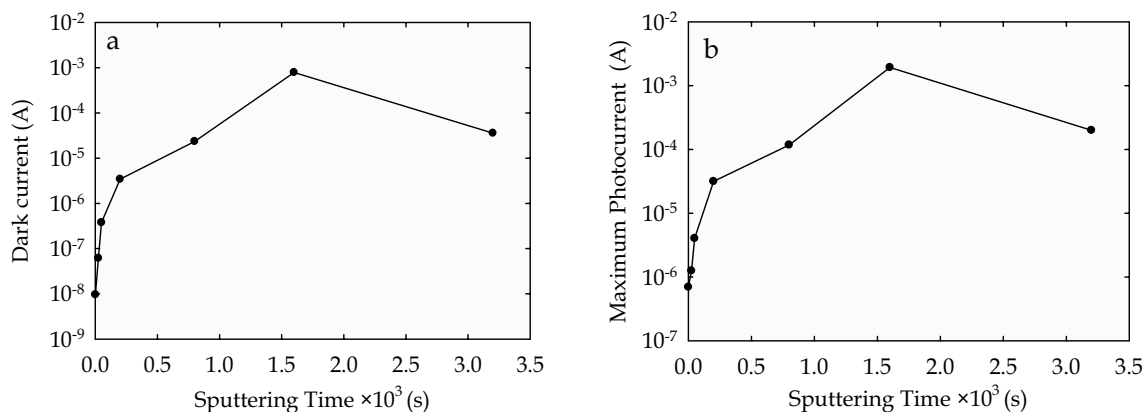


Fig. 8 **a** The dark current and **b** the maximum photocurrent of the sensors as a function of the sputtering time

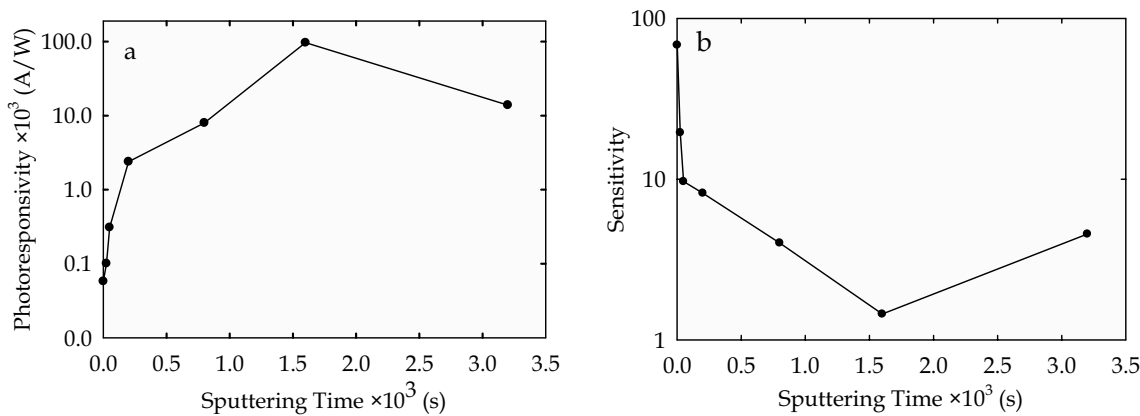


Fig. 9 a The photoresponsivity and b the sensitivity of the sensors as a function of the sputtering time

Figure 9a, b indicates variations of the photoresponsivity (R) and the sensitivity (S) of the sensors as a function of the sputtering time, respectively. According to the definition of R and the fact that the incident optical power on the sensor surface is constant, it is expected the photoresponsivity change curve will be very similar to the maximum current change curve when the UV light is on, which means that the parameter R is improved in doped sensors up to 1600 s sputtering time with Zr, whereas the sensitivity of the sensors is inversely related to the amount of doping up to 1600 s and is downward. In this case, reducing the sensitivity of the sensors with increasing the doping can readily be deduced from the fact that the growing rate of the dark current is higher compared with that of the maximum current when the UV light is on. The reason for this difference in the rate of current increase may be traced to the fact that the group of Zr atoms that replace Zn^{2+} in the form of Zr^{4+} on the surface of the ZnO layer not only increases the dark current by creating additional carriers, but also causes an increase in the photocurrent by interacting with further atoms of oxygen

when UV light is turned on and off. But another group of Zr atoms that are interstitially placed inside the ZnO lattice as the donor dopant increase the conductivity in the dark with increasing carriers while do not have much effect on increasing the photocurrent. Considering that the difference between the rate of increase in the dark current and the photocurrent is further observed with increasing doping rate, and the points mentioned in the analysis related to the reduction of the currents of sample g in high doping, one can conclude that, in the high doping regime, the presence manner of Zr atoms in the surface of zinc oxide layers changes from the Zr^{4+} substitution state instead of the Zn^{2+} atoms in the crystal surface to the interstitial state within the crystal lattice or their segregation at the surface grain boundaries.

Figure 10a, b illustrates the change of the rise and fall times of the sensors vs the sputtering time. In this research, the rise time is defined as the time interval corresponding to the photocurrent between 10% (or the minimum value if the initial value is more than 10%) and 90% of the maximum value; the fall time is expressed as the time interval corresponding to

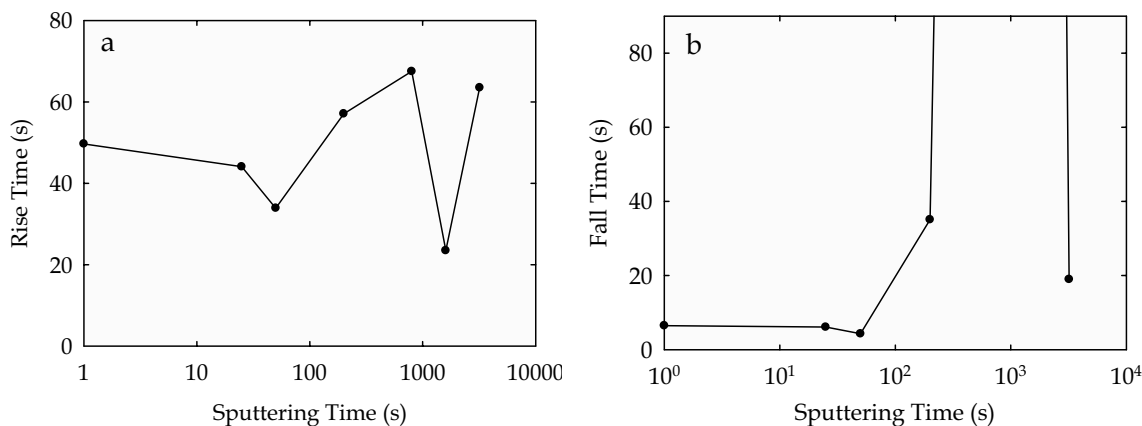


Fig. 10 The effect of the sputtering time on a the rise time and b the fall time of the sensors

Table 2 Comparison between different results related to some other MSM photodetectors with the one fabricated in this research

Nanostructure	Dopant	Bias voltage (V)	Rise time (s)	Fall time (s)	Photoresponsivity (A/W)	References
Thin film	Undoped	3	100	104	2.16	[41]
Thin film	Ag NP	30	15	330	2.86	[17]
Nanoflake	Al	10	>53	>107	0.0336	[42]
Thin film	rGO	2	44	40	–	[43]
Nanorod	Mn	5	27.07	>61.39	0.0765	[44]
Nanorod	Ga	1	>89	>106	0.046	[45]
Nanorod	Fe	3	46	37	0.758	[46]
Nanorod	Ni	3	70	43	2.10	[41]
Thin film	Zr	4	33.9	34.4	310	This work
Nanowire	Graphene	5	>11.9	>240	3.2×10^4	[47]

Here the rise time is defined as the time interval corresponding to the photocurrent between 10 and 90% of the maximum value; the fall time is expressed as the time interval corresponding to the photocurrent between the maximum and its 10% values

the photocurrent between the maximum and its $1/e$ values. In the rise time curve, there are two minimums: one for sample *c* with $t_s = 50$ s and another for sample *f* with $t_s = 1600$ s. For the latter, the minimum current value (the dark current) in the second cycle has increased to more than 50% of the maximum current value. The curve of recovery time (fall time) also shows that samples *e* and *f*, respectively, corresponding to $t_s = 800$ s and $t_s = 1600$ s have abnormal behavior, and their return time is too long (>1000 s). But the fall time of sample *c* with $t_s = 50$ s like its rise time is in the optimal situation (minimum). The reason for the reduction in these times is probably the easier exchange of ambient oxygen with new bonds created due to the replacement of Zr^{4+} ions with Zn^{2+} ions on the surface. With increasing the sputtering time, the probability of the presence of Zr atoms at greater depth and in other forms such as the interstitial state or even the segregated Zr and ZrO_2 increases, which can further slow the exchange of oxygen with the surface. From electrical point of view, the optimization of the response time of the MSM photodetector doped with Zr for 50 s sputtering time can be explained as follows. In the early stages of doping, an increase in dopants is concurrently accompanied with increasing carriers' density and mobility. Hence, both rise and fall times have a decreasing trend. This process continues until the sputtering time of 50 s. For more sputtering times, although carriers' density increases, due to the ionized impurity scattering phenomenon, the carriers' mobility eventually decreases and the response time becomes slower (as seen from Table 1). Therefore, one can say that the competition between two dominant physical phenomena, which are the mobility and the ionized impurity scattering, may be the main reason for establishing an optimized response time. The effect of doping Zr on increasing mobility has been also previously reported [24, 25].

In the end, it should be noted that so far numerous studies have been performed on the improvement and efficiency of MSM photodetectors based on ZnO nanostructures,

many of which have focused on improving response time and photoresponsivity [17, 41–47]. However, it is very difficult to compare the results of these studies with each other, because doping way and dopant type, the type and method of preparing the nanostructure, the material and shape of the electrodes, how the electrodes are made and the distance between them are all different in these research works. Furthermore, the test conditions particularly the radiated UV light power and the applied bias voltage are also different in various works. Consequently, for example, based on available reports, there is a difference in photoresponsivity up to seven order of magnitudes, and nevertheless, all of researchers assert that the performance of their detector has improved [48]. Therefore, it appears that, in these cases, the best way to evaluate the performance of each detector is to compare the results obtained for that detector before and after modifications, because other factors related to it can be kept invariant. However, the results of number of studies performed on the modification of ZnO-based MSM detectors using diverse dopants and various doping ways are presented in Table 2. Here, the response time and the photoresponsivity of some detectors with different nanostructure, dopant type, and also the bias voltage have been compared. Moreover, the mentioned results are related to the optimized detectors. As seen, these results reflect that photosensors fabricated in this research work have acceptable performance compared to the others in terms of response time and photoresponsivity.

4 Conclusion

In this research work, to make better the properties of ZnO-based MSM UV detectors, the surface of ZnO thin films prepared by sol–gel method was initially doped with Zr sputtering at time intervals of 25–3200 s. The amount of

Zr at the surface was evaluated by EDX spectroscopy and showed that the maximum ratio of Zr to Zn reaches 0.046 in 3200 s. AFM and XRD tests do not show much change in the morphology and crystal structure of the layers even after the most sputtering time, which is probably the reason that the major changes in this method occur only at a thickness of a few nanometers from the surface. By creating an electrode pair on the surface of each of the Zr-doped ZnO films, they were converted to MSM UV detectors and subjected to various sensor tests to assess their performance. The results of these tests showed that with increasing the sputtering time up to 50 s, most of the properties of the sensors improve, but after that time, the photoresponsivity, the sensitivity and the repeatability of $I-t$ curves of the sensors worsen drastically, and this is while, R continues to increase up to the sputtering time of 1600 s. This behavior appears to be due to the change in the preference of the presence of Zr atoms from the substitution state instead of Zn in the ZnO crystal lattice to the interstitial state between the lattice and segregated at the grain boundaries. Finally, it is important to note that, since the surface plays a major role in detection mechanisms in most light and gas sensors, the use of the sputtering method to modify the surface of the thin films used in the construction of sensors can much quickly and easily lead to the desired changes in detectors. In addition, this method can even be used to modify the properties of pre-made detectors.

References

1. F. Omnès, E. Monroy, E. Muñoz, J.-L.G. Reverchon, Nitride Mater. Dev. II Proc. SPIE **6473**, 64730 (2007)
2. S. Khan, D. Newport, S. Le Calvé, Sensors **19**, 5210 (2019)
3. Z. Xu, B.M. Sadler, IEEE Commun. Mag. **46**, 67 (2008)
4. A.P. Cracknell, C.A. Varotsos, Int. J. Remote Sens. **35**, 5566 (2014)
5. L. Sang, M. Liao, M. Sumiya, Sensors **13**, 10482 (2013)
6. T. Zhai, X. Fang, M. Liao, X. Xu, H. Zeng, B. Yoshio, D. Golberg, Sensors **9**, 6504 (2009)
7. Y. Zou, Y. Zhang, Y. Hu, H. Gu, Sensors **18**, 1 (2018)
8. K. Liu, M. Sakurai, M. Aono, Sensors **10**, 8604 (2010)
9. S.J. Young, L.W. Ji, R.W. Chuang, S.J. Chang, X.L. Du, Semicond. Sci. Technol. **21**, 1507 (2006)
10. K.J. Chen, F.Y. Hung, S.J. Chang, S.J. Young, J. Alloys Compd. **479**, 674 (2009)
11. S.J. Young, L.W. Jib, S.J. Chang, Y.K. Su, J. Cryst. Growth **293**, 43 (2006)
12. S.Z. Umbaidillah, N.A.M. Asib, A.N. Afaah, M. Rusop, Z. Khusaimi, AIP Conf. Proc. (2019). <https://doi.org/10.1063/1.5124668>
13. K.M. Sandeep, S. Bhat, S.M. Dharmaparakash, J. Phys. Chem. Solids **104**, 36 (2017)
14. S. Singh, Optik (Stuttg). **127**, 3523 (2016)
15. Z.N. Kayani, I. Shah, S. Riaz, S. Naseem, J. Mater. Sci. Mater. Electron. **28**, 5953 (2017)
16. H.S. Al-Salman, M.J. Abdullah, J. Mater. Sci. Technol. **29**, 1139 (2013)
17. X. Wang, K. Liu, X. Chen, B. Li, M. Jiang, Z. Zhang, H. Zhao, D. Shen, A.C.S. Appl. Mater. Interfaces **9**, 5574 (2017)
18. L. Xu, G. Zheng, Y. Liu, J. Su, W. Kuang, W. Rao, Optik (Stuttg) **147**, 6 (2017)
19. S. Roguai, A. Djelloul, Appl. Phys. A **126**, 1 (2020)
20. L. Ben Saad, L. Soltane, F. Sediri, Russ. J. Phys. Chem. A **93**, 2782 (2019)
21. D. Chakraborty, R. Gayen, S. Hussain, R. Bhar, A.K. Ghoshal, A.K. Pal, J. Phys. Conf. Ser. **390**, 1 (2012)
22. A. Jamil, S. Fareed, N. Tiwari, C. Li, B. Cheng, X. Xu, M.A. Rafiq, Appl. Phys. A **125**, 1 (2019)
23. K. Bahedia, M. Addoua, M. El Jouada, Z. Sofiania, S. Bayouda, B. Sahraoui, Z. Essaidi, ICTON-MW (2008). <https://doi.org/10.1109/ICTONMW.2008.4773058>
24. C.Y. Tsay, K.S. Fan, Mater. Trans. **49**, 1900 (2008)
25. G.K. Paul, S. Bandyopadhyay, S.K. Sen, S. Sen, Mater. Chem. Phys. **79**, 71 (2003)
26. M. Lv, X. Xiu, Z. Pang, Y. Dai, L. Ye, C. Cheng, S. Han, Thin Solid Films **516**, 2017 (2008)
27. M. Lin, Y. Chang, M. Chen, C. Chu, J. Electrochem. Soc **158**, 395 (2011)
28. S. Huber, C.C. Mardare, A.I. Mardare, C. Kleber, A.W. Hassel, RSC Adv. **9**, 35579 (2019)
29. U. Demirkol, S. Pat, R. Mohammadigharehbagh, C. Musaoğlu, M. Özgür, S. Elmas, S. Özen, Ş Korkmaz, J. Mater. Sci. Mater. Electron. **29**, 18098 (2018)
30. I. Khan, S. Khan, R. Nongjai, H. Ahmed, W. Khan, Opt. Mater. (Amst). **35**, 1189 (2013)
31. N.C.S. Selvam, J.J. Vijaya, L.J. Kennedy, Ind. Eng. Chem. Res. **51**, 16333 (2012)
32. J. Zhang, D. Gao, G. Yang, J. Zhang, Z. Shi, Z. Zhang, Z. Zhu, D. Xue, Nanoscale Res. Lett. **6**, 1 (2011)
33. V. Gokulakrishnan, S. Parthiban, K. Jeganathan, K. Ramamurthi, Appl. Surf. Sci. **257**, 9068 (2011)
34. R. Khokhra, B. Bharti, H.-N. Lee, R. Kumar, Sci. Rep **7**, 15032 (2017)
35. Z. Huaifu, L. Chengxin, L. Hanfa, Y. Changkun, J. Semicond. **30**, 043004–043011 (2009)
36. S. Herodotou, R.E. Treharne, K. Durose, G.J. Tatlock, R.J. Potter, Materials **8**, 7230 (2015)
37. L. Mao-Shui, P. Zhi-Yong, X. Xian-Wu, D. Ying, H. Sheng-Hao, C. Phys. **16**, 548 (2007)
38. Z. Ye, H. Lu, Y. Geng, Y. Gu, Z. Xie, Y. Zhang, Q. Sun, S. Ding, D. Zhang, Nanoscale Res. Lett. **8**, 1 (2013)
39. T. Minami, H. Sato, H. Nanto, S. Takata, Jpn. J. Appl. Phys. **24**, 781 (1985)
40. M.C. Jun, S.U. Park, J.H. Koh, Nanoscale Res. Lett. **7**, 1 (2012)
41. Y.-L. Chu et al., J. Electrochem. Soc. **167**, 067506 (2020)
42. M.H. Mamat, Z. Khusaimi, M.Z. Musa, M.F. Malek, M. Rusop, Sens. Actuat. A Phys **171**, 241 (2011)
43. S. Safa, R. Sarraf-Mamoory, R. Azimirad, Physica E **57**, 155 (2014)
44. H.A. Alshamarti, A.H.O. Alkhayatt, Mater. Sci. Semicond. Process. **114**, 105068 (2020)
45. S.-J. Young, Y.-H. Liu, M.D.N.I. Shiblee, K. Ahmed, L.-T. Lai, L. Nagahara, T. Thundat, T. Yoshida, S. Arya, H. Furukawa, A. Khosla, A.C.S. Appl. Electron. Mater. **2**, 3522 (2020)
46. Y.-L. Chu, S.-J. Young, L.-W. Ji, I.-T. Tang, T.-T. Chu, Sensors **20**, 3861 (2020)
47. B.D. Boruah, D.B. Ferry, A. Mukherjee, A. Misra, Nanotechnology **26**, 235703 (2015)
48. B.D. Boruah, Nanoscale Adv. **1**, 2059 (2019)

Publisher's Note Springer Nature remains neutral with regard to jurisdictional claims in published maps and institutional affiliations.